Electronic Supplementary Material (ESI) for Nanoscale.

Supplemental Material

Unconventional magnetic anisotropy in one-dimensional Rashba system realized by adsorbing Gd atom on zigzag graphene nanoribbons

Zhenzhen Qin[1] , Guangzhao Qin[2] , Bin Shao[3], Xu Zuo[1*]

[1] *College of Electronic Information and Optical Engineering,*

Nankai University, Tianjin, 300350, China

[2] *Institute of Mineral Engineering, Division of Materials Science and Engineering,*

Faculty of Georesources and Materials Engineering,

RWTH Aachen University, Aachen 52064, Germany

[3] *Bremen Center for Computational Material Science,*

Bremen University, Am Fallturm 1, Bremen 28359, Germany

Email: xzuo@nankai.edu.cn

(a) Electronic structure of pure zizag graphene nanoribbon

* To whom correspondence should be addressed.

Fig. S1 gives the structure, sin density and band structures of pure 4ZGNR. From Fig. S1(b), it is clearly see that spin moments are mainly distributed at the edge carbon atoms and slower decay towards the center of the ribbon. The magnetic moment fluctuation across the ribbon arises from quantum interference effects caused by nanoribbon edges. Due to topology of the lattice, the atoms of the two edges belong to different sublattices of the bipartite graphene lattice. The spin density on the C atoms on one edge are antialigned to the spin density on the opposite edge, and the polarizations of neighboring sites belonging to different sublattices are also opposite. The band structure of ZGNR decorated with up/down C-p_z orbitals is presented in Fig. S1(c) respectively.

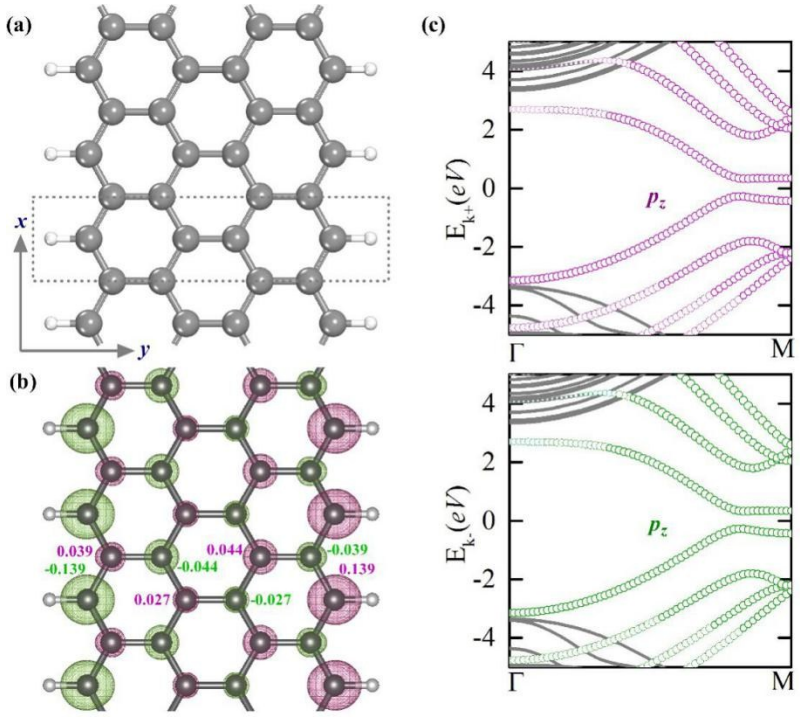

Figure S1. Structure of H-passivated 4-ZGNR, where the gray and white balls represent C and H atoms, respectively. The unit cells are indicated by dashed lines. (b) Spin up (red gray) and down (green gray) density plots of pure 4-ZGNR (2×10^{-3}e/Å^3) showing together with the corresponding values of local magnetic moments. (c) Spin up (red gray)/down (green gray) bands of 4ZGNR showing the amplitudes of the projection band of p_z orbital of edge carbon atoms.

(b) Orbital-projected density of states of Gd-ZGNR

We provide the orbital-projected density of states of Gd-ZGNR at h_1 site, and give that of h_2 site for comparison, as shown in Fig. S2. It is found that the orbital splitting of Gd-5*d* levels are almost no difference in the two adsorbed cases: The down-spin density of Gd-*d* orbitals are all empty, while the up-spin density reveals that d_{xy}, d_{yz}, d_{xz} orbitals are nearly unoccupied, which lie higher in energy than the obvious partially filled dx^2-y^2 and dz^2 orbitals.

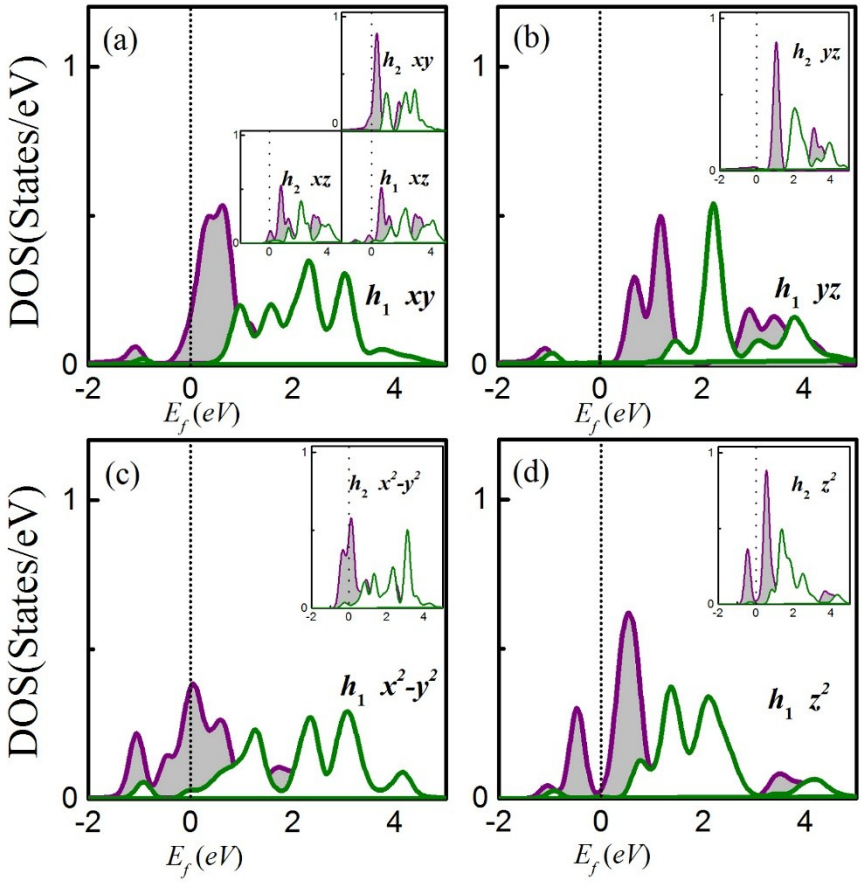

Figure S2. The orbital-projected densities of states of Gd adatom at h_1 position in ZGNR. Insets of (a-d) present *d*-DOS of Gd adatom at h_2 site. And insets of (a) provides the d_{xz} partial DOS of Gd adatom at h_1 site. Red gray region denotes spin-up contributions and green blank the spin-down contributions.

(c) Pseudo gap in h_1-Gd-ZGNR

Due to the pseudo-gap is enlarged at Γ point in the perturbed band structures of h_1-Gd-ZGNRs, we prove that relationship from the first-order perturbation of the SOC interaction, $H_{SOC} = \xi l \cdot s = \xi(l_x \sin\theta + l_z \cos\theta)s$, where we assume that the spin is in the *xz*-plane, here $s = 1/2$, ξ is the effective SOC interaction constant, and θ is the angle between the spin-axis and the *z*-axis. Because the two separated orbitals at Γ point are d_{xy} and $d_{x^2-y^2}$, so we can directly write the matrix representation

$$H_{SOC} = \frac{\xi}{2}\cos\theta \begin{pmatrix} \varepsilon & -2i \\ 2i & \varepsilon + \Delta \end{pmatrix}, \tag{1}$$

where ε and $\varepsilon + \Delta$ are the two levels before perturbation at Γ point.

Set the $h = \xi \cos\theta$, it can be written as

$$\begin{pmatrix} \varepsilon & -ih \\ ih & \varepsilon + \Delta \end{pmatrix}, \tag{2}$$

Diagonalizing this matrix, we obtain two levels after perturbation

$$\lambda_{\pm} = \frac{2\varepsilon + \Delta \pm \sqrt{\Delta^2 + 4h^2}}{2}, \tag{3}$$

and the gap after perturbation

$$\Delta_\theta = \sqrt{\Delta^2 + 4h^2} = \Delta\sqrt{1 + 4\left(\frac{h}{\Delta}\right)^2}. \tag{4}$$

When $h << \Delta$, $\Delta_\theta \approx \Delta\left(1 + 2\left(\frac{h}{\Delta}\right)^2\right)$, and when $h >> \Delta$, $\Delta_\theta \approx 2h$. Note that $h \propto \cos\theta$, when the polar angle θ is close to 90, the gap is proportional to $(\cos\theta)^2$, and when θ~0°, the gap is proportional to $\cos\theta$.

(d) Band structures of h_2-Gd-ZGNR perturbed with SOC

The band structures for h_2-Gd-4ZGNR in different magnetization directions is provided in Fig. S3. Observed from the band structures with the perpendicular (001) and $(00\bar{1})$ magnetization, it is clearly shown that there is no movement which turn out that the non-existed offsetting first-order perturbation contribution, consistent with the MAE contributions along *k*-line.

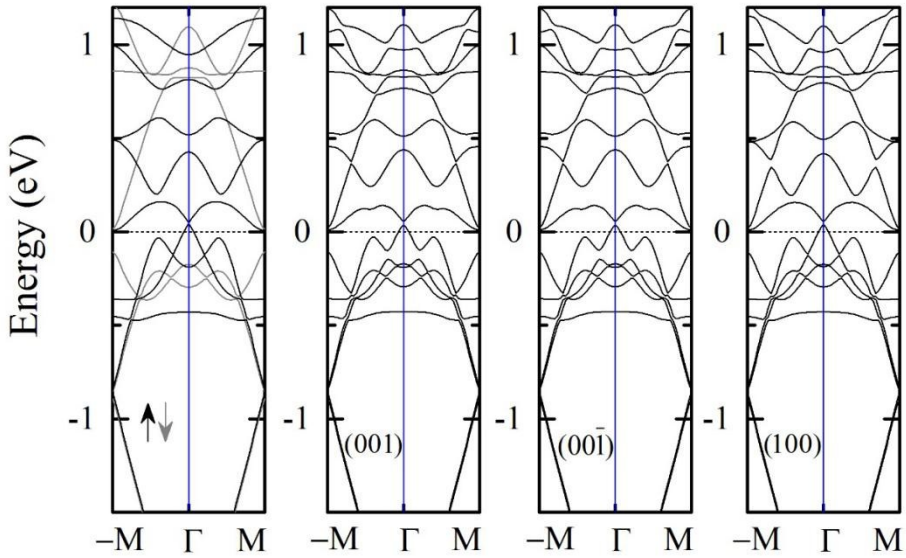

Figure S3. (a) The band structure in the first Brillouin zone(−M~Γ~M) of non-perturbed and perturbed with the (001), (100) and (00-1) magnetization for Gd-4ZGNR at h_2 site, respectively. The Fermi energy is set as zero.

(e) Rashba parameter

The Rashba Hamiltonian is $H = \alpha\sigma(k_x \times e_z)$, here, α is the Rashba parameter which represents strength of Rashba effect, σ is the Pauli matrix, k_x the in-plane momentum, e_z is the surface normal vector. Due to spin-orbital coupling, the spin splitting of band structure could be described by:

$$E^{\pm}(k) = \frac{\hbar^2}{2m^*}\vec{k_x}^2 \pm \alpha\vec{k_x} \quad (5)$$

where m^* represents the electron effective mass.

The Eq. (5) can be written as

$$E^{\pm}(k) = \frac{\hbar^2}{2m^*}\left(k_x \pm \frac{m^*\alpha}{\hbar^2}\right)^2 - \frac{m^*\alpha^2}{2\hbar^2} \quad (6)$$

Thus, the momentum splitting of the Rashba bands from the crossing point is defined as $\Delta k_R = \frac{m^*\alpha}{\hbar^2}$. Finally, the Rashba parameter could be deduced as $\alpha = \hbar^2\Delta k_R / m^*$.

(f) The possible adsorption sites of Gd adsorbed *n*-ZGNRs

The possible adsorption hollow sites of Gd adsorbed *n*-ZGNR (*n*=5, 6, 7, 8, 9, 10, 12) are provide in Fig. S4. In addition, the energy differences among the antiferromagnetic (AFM), ferromagnetic (FM), nonmagnetic (NM) states of *n*-ZGNRs (*n*=5, 6, 7, 8, 9, 10, 12) are given as E_{AFM-FM} and E_{AFM-NM} in Table S1. Our calculated values are in good agreement with previous results reported by Krychowski et. al[1].

TABLE S1. Energy differences among the antiferromagnetic (AFM), ferromagnetic (FM), nonmagnetic (NM) states of *n*-ZGNRs (*n*=5, 6, 7, 8, 9, 10, 12). The results reported by Krychowski et. al[1] are also provided.

n	E_{AFM-FM} (meV)		E_{AFM-NM} (meV)	
	This work	Others[1]	This work	Others[1]
5	-10.85	-10.67	-64.32	-65.10
6	-11.68	-11.39	-68.56	-69.41
7	-10.33	-8.83	-77.62	-71.64
8	-7.735	-5.88	-72.83	-73.73
9	-6.78	-4.23	-78.59	-75.75
10	-6.42	-3.34	-75.837	-77.47
12	-2.59		-78.42	

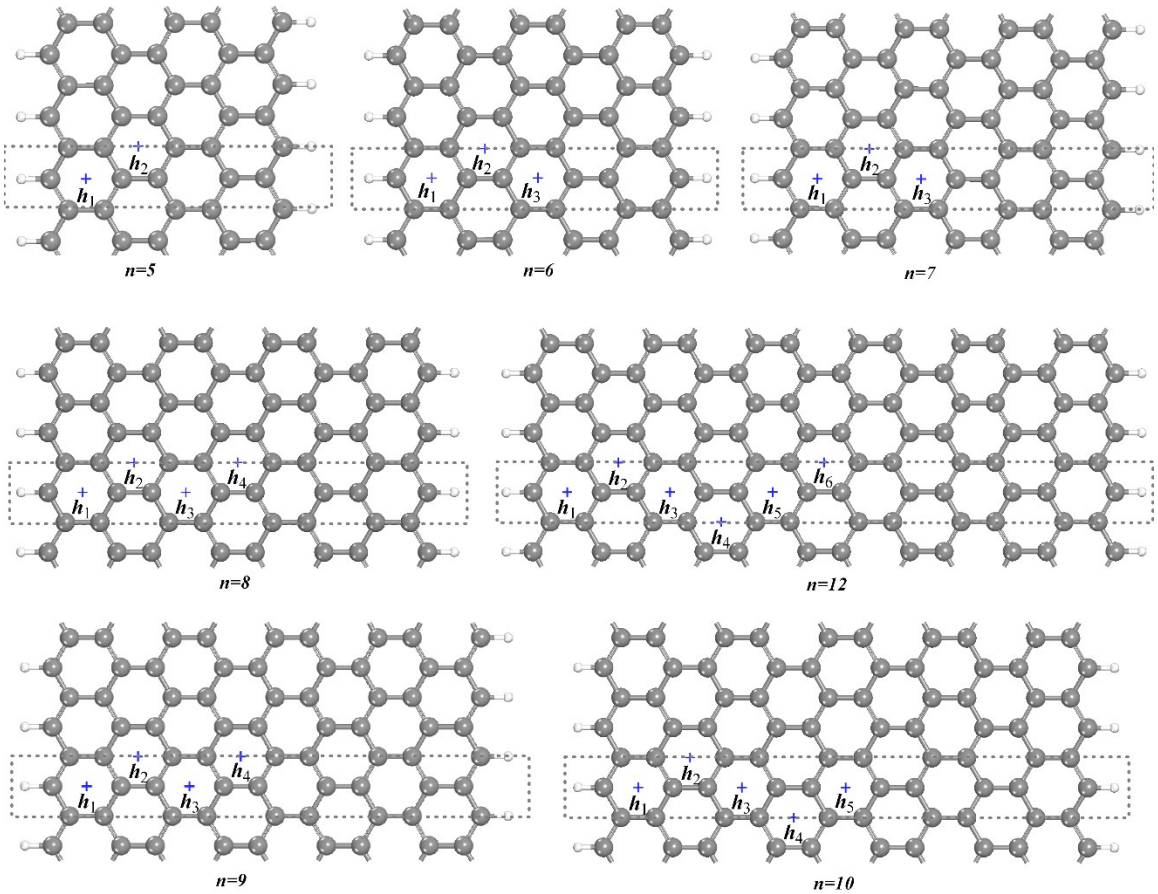

Figure S4. (a) Structures of *n*-ZGNRs with the width *n*= 5, 6, 7, 8, 9, 10, 12. The inequivalence possible hollow sites are labeled for Gd-*n*ZGNRs (*n*= 5, 6, 7, 8, 9, 10, 12) respectively. Such as, for the 12-ZGNR, there are six possible adsorption hollow sites (h_1, h_2, h_3, h_4, h_5, h_6).

References

[1] D. Krychowski, J. Kaczkowski, and S. Lipinski, *Phys. Rev. B* **89**, 35424 (2014).